Timing

Andrea Grossutti, mat. 1237344
Alessandro Lovo, mat. 1236048
Leonardo Zampieri, mat. 1237351

December 1, 2019

1 Aims

- Energy calibration of the organic scintillators and calculation of the energy resolution from the analysis of the Compton edge;
- Optimization of the external delay of the analogue CFTD to obtain the best time resolution;
- Study of the time resolution behaviour as a function of the energy;
- Comparison between the timing resolutions obtained from analogue and digital treatment of the signals;
- Measurement of the speed of light.

2 Experimental setup

The experimental setup consist of two collinear organic scintillators (DET 1 and DET 2), mounted on a sledge and facing each other. Between them there is a ^{22}Na source collimated by two lead bricks. The energy peaks of photons emitted by this source are shown in tab 1.

photopeak [keV]	Compton Edge [keV]
511.0	340.7
1274.537	1061.7

Table 1: Gamma radiation for ^{22}Na from NuDat, `https://www.nndc.bnl.gov/nudat2/decaysearchdirect.jsp?nuc=22NA&unc=nds`

Data are collected from the detectors through a electronic chain: a fan-in-fan-out quad module replies the signal of each detector and produces four replies of it; then, through a Constant Fraction Time Discriminator (CFTD), a logic signal is produced. The CFTD trigger threshold has been set so that the noise is discarded, while the interesting signals produce an output. From the CFTD the logic signal runs through a coincidence unit, used as a trigger. Besides, the logic signal of DET 1 runs into the *start* of a Time to Amplitude Converter (TAC) module, while the one from DET 2 passes through a delay module and then runs into the *stop* of the TAC. A digitizer, triggered by the coincidence unit, acquires the energy spectra of both detectors and the time spectrum of the TAC.

3 Apparatus calibration

3.1 Calibration of detectors

Disabling the coincidence unit in order to collect both peaks of the ^{22}Na source, a spectrum for each detector is acquired. Due to the chemical composition of the detector (low Z materials), photopeaks are negligible and only the Compton effect is detected.

The observed Compton Edge (CE) is a convolution of the real CE with a gaussian noise $\mathcal{N}(0, \sigma_{res})$ due to the detector finite resolution; this convolution results in a shift of the maximum of the CE towards lower energies. So, in order to calibrate the detectors, an estimate of this shift is needed.

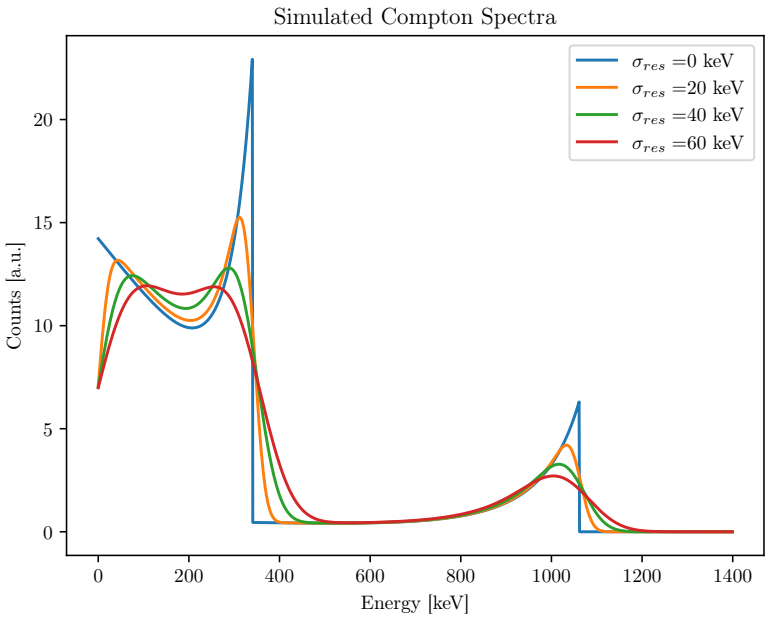

Figure 1: Simulated Compton spectra with different values of σ_{res}. Even if here the two peaks are represented together, they were analized independently.

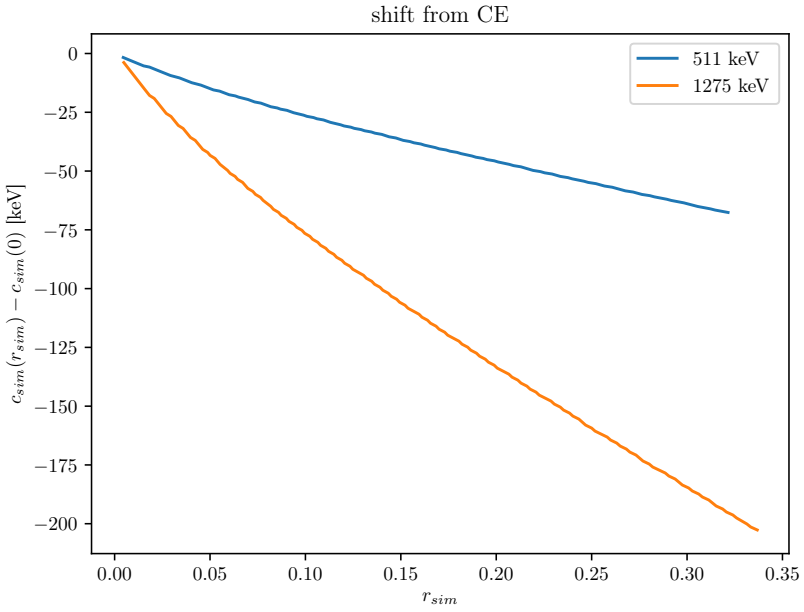

Figure 2: Relation between the resolution of the peak and the peak position, in calibrated histograms.

By simulating* the effects on CE varying σ_{res} (fig 1) the position of the peak c_{sim} and its right Half Width Half Maximum w_{sim}† can be computed, and the correlation between simulated resolution

*For formulas see N. Kudomi *Energy calibration of plastic scintillators for low energy electrons by using Compton scattering of γ rays*, Nuc. Instr. and Meth., 430 (1999), `https://doi.org/10.1016/S0168-9002(99)00200-4`

†We used this approach instead of a gaussian fit of the peaks because both in the simulation and in the experimental

$r_{sim} = \frac{w_{sim}}{c_{sim}}$ and c_{sim} can be studied (fig 2).

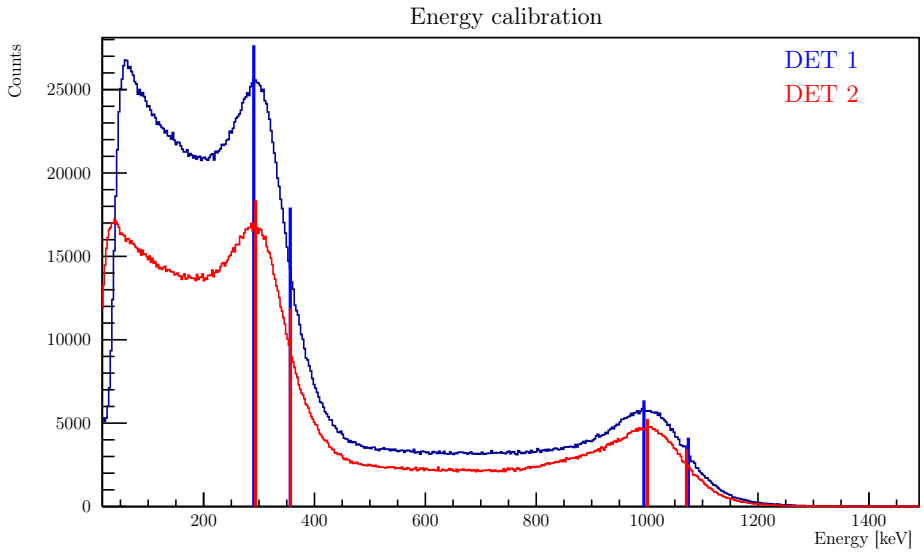

Figure 3: Position of CE's centroids and widths

Det	p [keV]	c_{ch}	w_{ch}	c_E [keV]	w_E [keV]	r_E	σ_{res} [keV]
#1	511	3440 ± 9	736 ± 13	290.2 ± 0.7	66 ± 1	0.227 ± 0.004	38.8 ± 0.5
	1275	11312 ± 9	960 ± 13	994.1 ± 0.8	225 ± 4	0.086 ± 0.001	37.0 ± 0.5
#2	511	4400 ± 9	768 ± 13	293.8 ± 0.7	60 ± 1	0.205 ± 0.004	35.7 ± 0.6
	1275	13392 ± 9	960 ± 13	1000.5 ± 0.7	206 ± 4	0.075 ± 0.001	33.9 ± 0.5

Table 2: Centroids and widths of the CE peaks: p is the photopeak energy. The errors for the values in channels come from a uniform distribution on the bin width of the histogram. The values of c_E, w_E, r_E and σ_{res} here are the ones after the calibration process converged.

Computing c_{ch} and w_{ch} for the experimental spectra in channels (fig 3, tab 2), noting that for the peak relative to the 511 keV photon the half maximum needs to be computed with respect to the baseline due to the low energy Compton events of the 1275 keV photon, the calibration of the energy spectra can be done.
Assuming a calibration relation $E = a \cdot \mathrm{ch} + b$, the resolution in energy is:

$$r_E = \frac{w_E}{c_E} = \frac{a w_{ch}}{a c_{ch} + b} = \frac{w_{ch}}{c_{ch} + b/a}$$

Starting from $b/a = 0$, imposing $r_E = r_{sim}$ and iterating updating b/a ratio until the process converges, the results in tab 3 can be found.

Det	a [keV]	b [keV]
#1	0.0894 ± 0.0002	-17 ± 2
#2	0.0786 ± 0.0002	-52 ± 2

Table 3: Calibrations coefficients after the calibration process converged.

spectra the result of the fit was highly dependent on the range chosen for the fit, which is arbitrary. See also Dietze, Klein: *Gamma-calibration of NE 213 scintillation counters*, Nuc. Instr. and Meth., 193 (1982), `https://doi.org/10.1016/0029-554X(82)90249-X`

3.2 Calibration of the TAC

By changing the delay of the delay module just before the TAC's *stop*, we can acquire different TAC peaks and use them for calibration (fig 4). For each peak the centroid is found through gaussian fit on a small range around the maximum (tab 4).

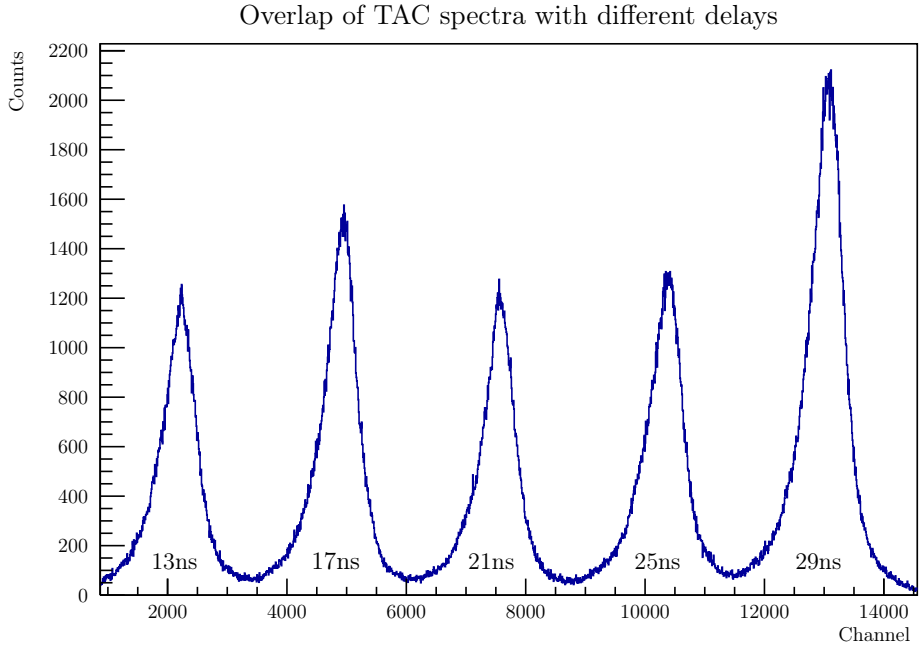

Figure 4: Different peaks with different delays. Different height of the peaks are due to different acquisition time.

Delay [ns]	Centroid [channel]
13	2235 ± 20
17	4950 ± 30
21	7555 ± 30
25	10390 ± 30
29	13080 ± 40

Table 4: TAC centroids.

The centroids are fitted using a linear relation:

$$t = m \cdot \mathrm{ch} + q$$
$$m = (1.477 \pm 0.005)\mathrm{ps} \qquad \chi^2/\mathrm{ndf} = 11/3$$

where the q value isn't reported, having no meaning. In fact, delays are introduced in a more complex system, which already have an intrinsic delay: zero external delay therefore doesn't mean zero time in TAC.

4 LEMO calibration

A set of LEMO cables is provided. Setting external delay to 13ns and inserting one by one each LEMO cable in series with the external delay module, 5-minutes datasets are acquired; computing the difference between the observed centroids and the centroid without LEMO cable previously measured, and converting it with the calibration parameter, the time-length of each LEMO cable is computed.

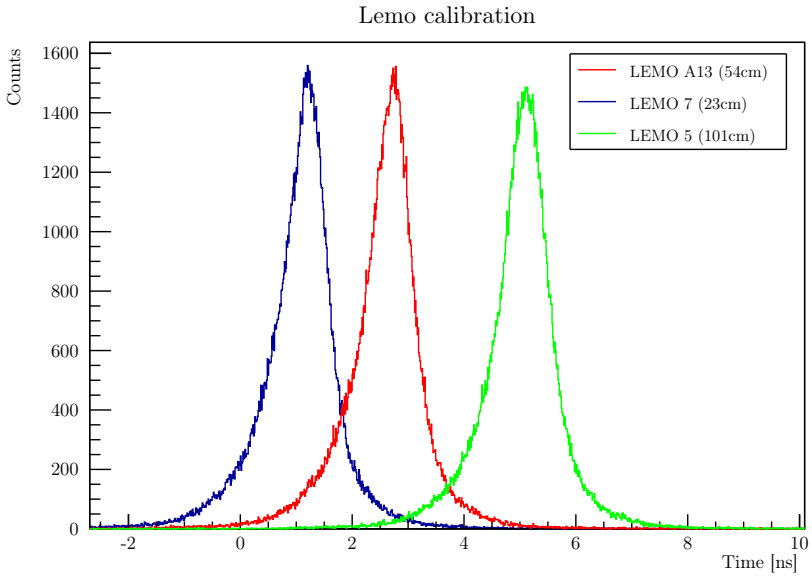

Figure 5: Some of the peaks of the LEMO cables

LEMO ID	LEMO length [cm], ±0.1	LEMO time [ns]
6	22.5	1.17 ± 0.04
7	23.0	1.15 ± 0.04
2	53.5	2.70 ± 0.03
13	53.5	2.71 ± 0.05
4	101.0	5.12 ± 0.04
5	101.0	5.08 ± 0.07

Table 5: LEMO cables

The time length of each LEMO cable can be compared with it's metric length, finding a linear relation as expected.

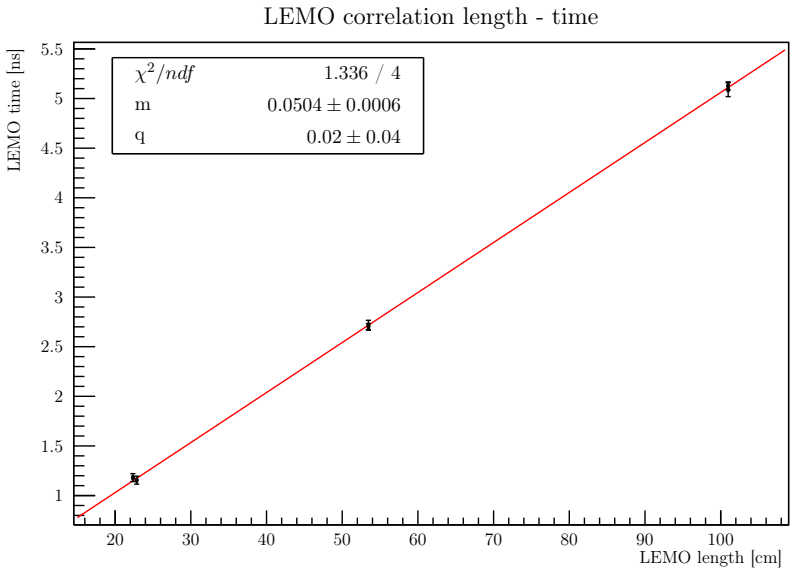

Figure 6: Relation between LEMO length and time: as expected, the dependence is confirmed.

5 CFTD delay optimization

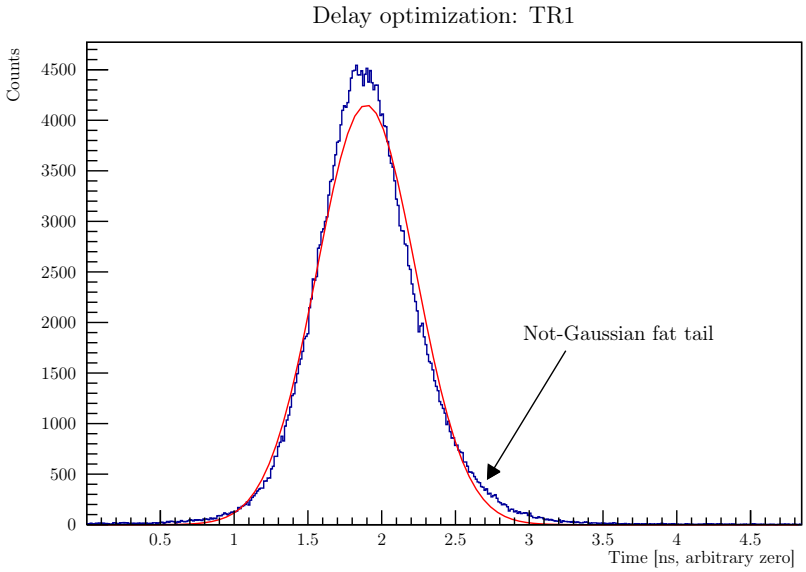

Figure 7: Initial situation: large not-guassian shape.

The CFTD superimposes a delayed copy of the signal to an inverted attenuated one. This delay must be properly set using LEMO cables to optimize the TAC resolution. With only the default delay, the signal detected by the TAC is large and not gaussian (see fig. 7); after some tests, a setup which lead to a better resolution and a more gaussian-like output is obtained.

Different combination of LEMO cable have been inserted in series with the pre-set delay; every time the configuration changed, the WALK ADJ potentiometer has been regulated to minimize the dispersion (see fig. 8) at the zero-crossing point of the signals.

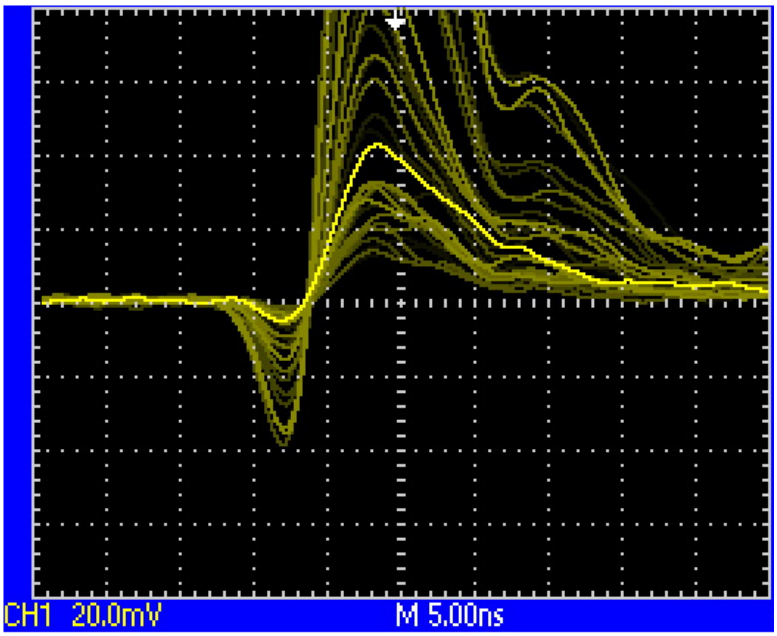

Figure 8: Monitor CFTD signal triggered on CFTD output, seen by the oscilloscope.

Fitting the obtained peaks with a gaussian and relating them to the delay inserted in the CFTDs (after some tests, we noticed that the optimal setup is with the same delay in both CFTDs), we obtain the result in fig 9. As can be seen from the figure, a minimum is found at about 3ns of delay (LEMO 13 for DET 1 and LEMO 2 for DET 2). Considering the pre-set delay (around 2ns), this lead to a

optimal delay of around 5ns, that is about 80% (one minus the attenuation fraction) the rise time of the detector signal ($\sim$ 6ns), as theoretically expected.

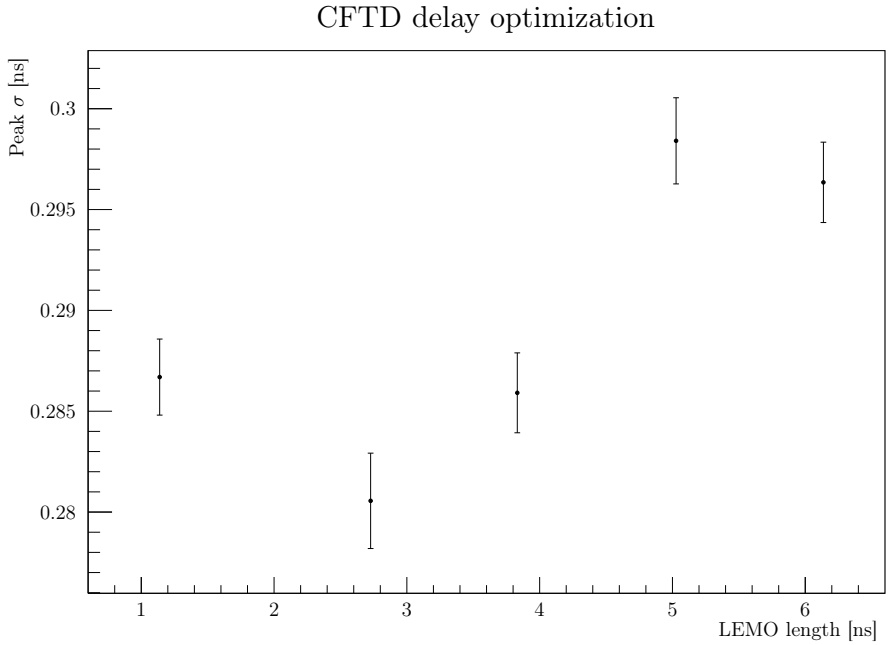

Figure 9: Optimization of the CFTD delay.

The minimum configuration has been kept for all the following measurements.

6 Time resolution in function of energy range

In order to have a wider Compton energy spectra, 20 hours of data are acquired using a ^{60}Co source. This source decays emitting two photons of energy around 1MeV: a few of them are emitted back-to-back and hence can trigger the coincidence unit (fig 10), that is set in *AND* configuration.

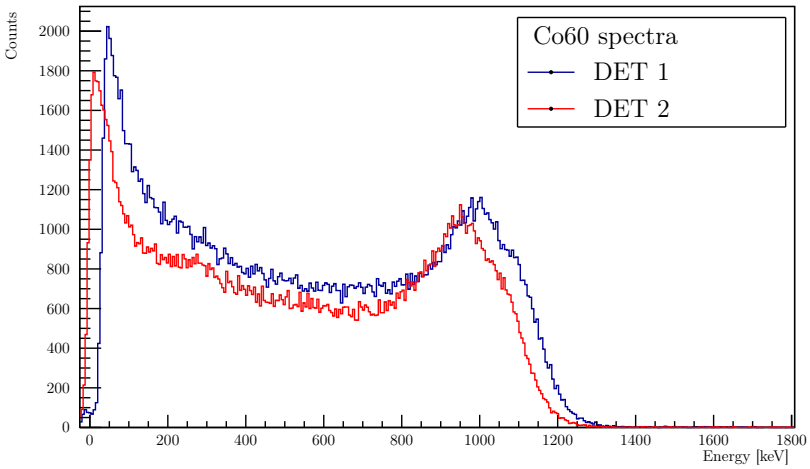

Figure 10: Energy spectra of the two detectors with ^{60}Co source.

Properly filtering in energy the spectra, the dependence of the resolution of the TAC can be studied. Since, despite the delay optimization, the TAC peaks still have a slightly fat-tailed distribution, the gaussian fit is not accurate. Therefore, the Full Width Half Maximum (FWHM) is used. The filtering

can be done either by setting a Lower Energy Threshold (LET) or by selecting a window in energy, i.e. keeping only the data with energy between the LET and an Upper Energy Threshold (UET). The results are shown in fig 11.

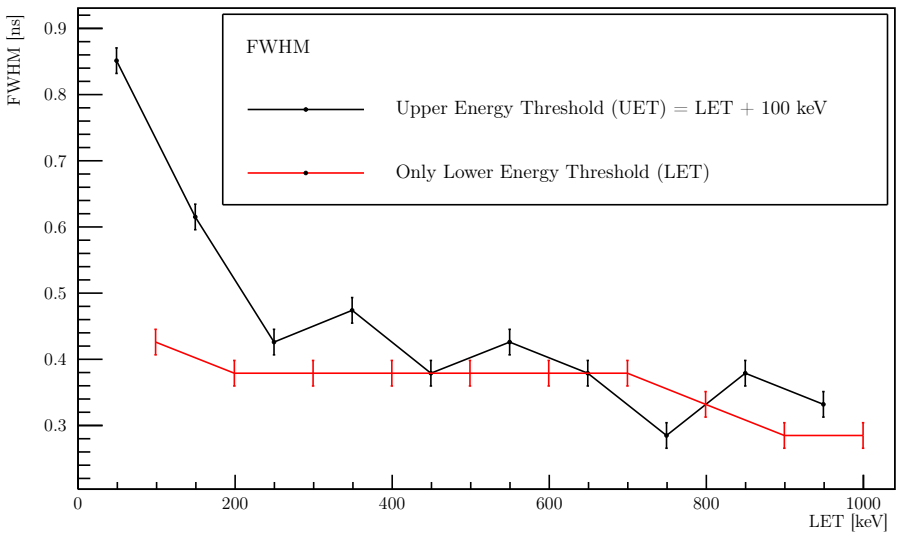

Figure 11: When computing the FWHM, the peaks had been properly rebinned in order to have them sufficiently smooth. The errors on the FWHMs come from a uniform distribution on the bin width.

From fig 11 we can see the resolution improves dramatically as we discard the events at lower energy, and then keep to slowly improve as LET increases. An equilibrium must be found between discarding low energy events with poor time resolution and keeping enough events to have a rich statistic. This equilibrium strongly depend from from the shape and the width of the source energetic spectra.

7 Speed of light

The detectors have been placed such that they're about 1.70m away. The ^{22}Na source has been placed firstly near DET 1 and then near DET 2, and the TAC signal has been acquired (one hour for each configuration); then, the centroids μ_1 and μ_2 of the two measurements have been found through a gaussian interpolation. Measuring the distance between the two source positions d, the light speed can be computed.

Observe that the two centroids have been firstly subtracted keeping them in channel and then calibrated, to prevent the introduction of correlation between the two measures.

The errors have been propagated as statistical errors. Note the high error on the distance between the positions of the source, due to the width of the source itself.

$$\mu_1 = (16433 \pm 5)\text{channel}$$
$$\mu_2 = (8966 \pm 5)\text{channel}$$
$$d = (162 \pm 1)\text{cm}$$
$$c = \frac{2d}{(\mu_1 - \mu_2)m} = (2.94 \pm 0.02) \cdot 10^8 \text{m}\,\text{s}^{-1}$$

which is compatible with the true value.

8 A-Posteriori CFTD

@Leonardo: riletto fin qui

During the last day, we disabled the digitizer's FPGA and acquired two datasets of raw waveforms directly from the detectors. This allows us to simulate an a-posteriori software CFTD, and compare it with the analogic one.

8.1 Waveforms

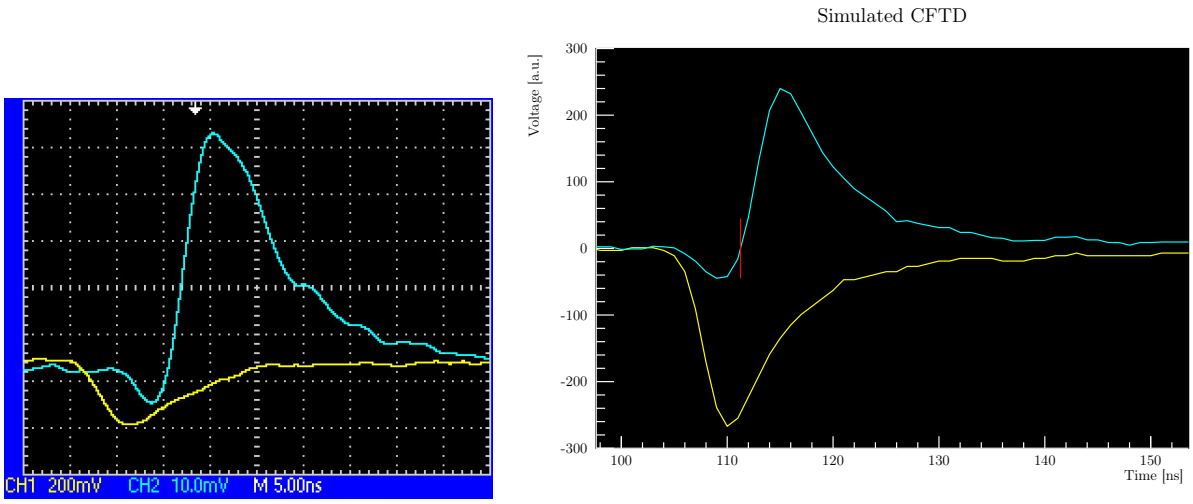

(a) Analogic CFTD

(b) APosteriori CFTD

Figure 12: Waveforms (yellow) and monitor signals (cyan) for analogic and software CFTD, set with the same parameters (fraction = 20%, delay = $\sim$ 5ns)

As can be seen from fig. 12, the shape of waveform and signal is similar for the two system. Rise time (about 6ns) and falling time (about 20ns) are the same. The signal, however, is very short in time and the low time resolution of the digitizer (a sample each 1ns) result in a rougher waveform.

8.2 Energy spectra

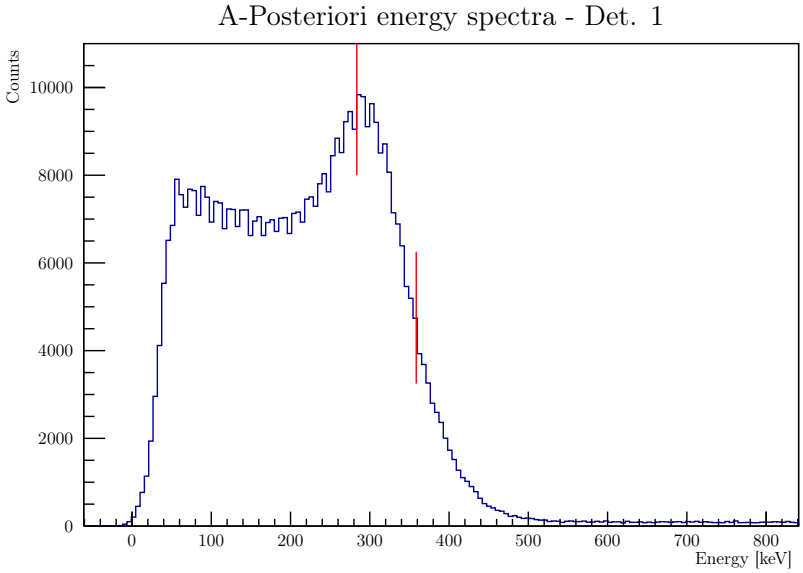

Figure 13: APosteriori energy spectra.

Si potrebbe sovrapporre lo spettro analogico (eventualmente normalizzando i due istogrammi)

Integrating the waveform (substracted of the baseline) over the domain, an energy spectra can be computed. As can be seen comparing fig. 13 with fig. 3, here only the 511keV peak is visible: the trigger set on coincidences and the low acceptance of the digitized cut away the higher peak.

Even with only one peaks, the comparison with the previous calibration permit us to make a rough calibration using position of peak and half maximum (in red in figure).

Note that in this plot there are some energy that are below zero; this is due to the combination between the low trigger threshold and the detectors resolution, the convolution of which result in a tail in negative energies.

8.3 CFTD parameters

For each dataset, the following procedure is followed:

- Coincidences are searched, i.e. events that are recorded by both the detectors;
- For each event, a simulated CFTD is applied to the two waveforms and zero crossing are computed;
- For each event, the time difference between the zero crossings in the two detector is computed;
- The distribution of the time difference is builded: mean, sigma (defined as the square root of the normalized centered second moment of data) and kurtosis (a measure of the *gaussianity* of the distribution) are computed;

This procedure is repeated for different combination of CFTD delay (from 1 to 10ns, with 0.25ns step) and attenuation fraction (from 0.1 to 0.9, with 0.1 step) and the plots of sigma and kurtosis are builded.

Io farei i due grafici seguenti usando lo stesso colore per valori belli (es. rosso) e lo stesso per valori brutti (es. blu). Può essere che sia già così e che io non abbia capito come funziona il Kurtosis e/o perché abbia valori negativi oggi (ieri eran positivi). Ma sono abbastanza sicuro di avere ragione e che quindi sia carino invertire i colori di uno dei due.

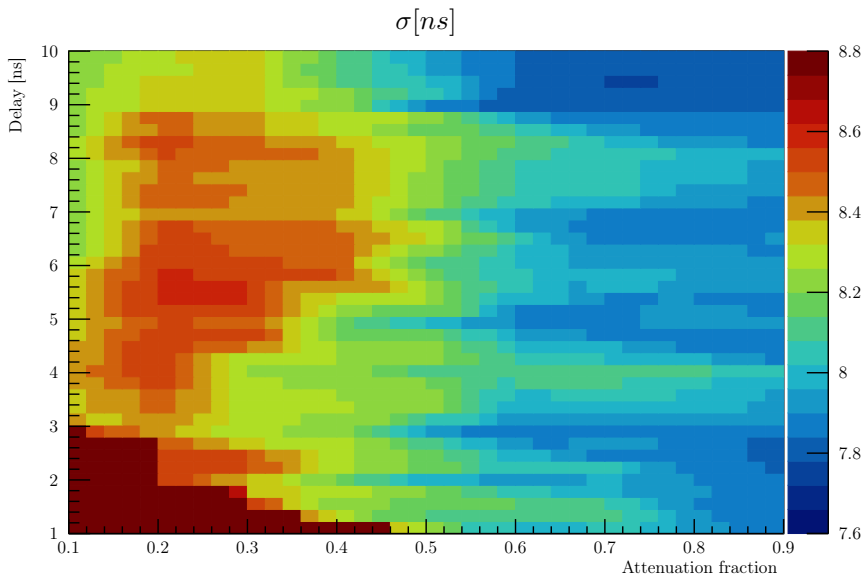

Figure 14: Sigma of the time differences distribution as function of CFTD parameters.

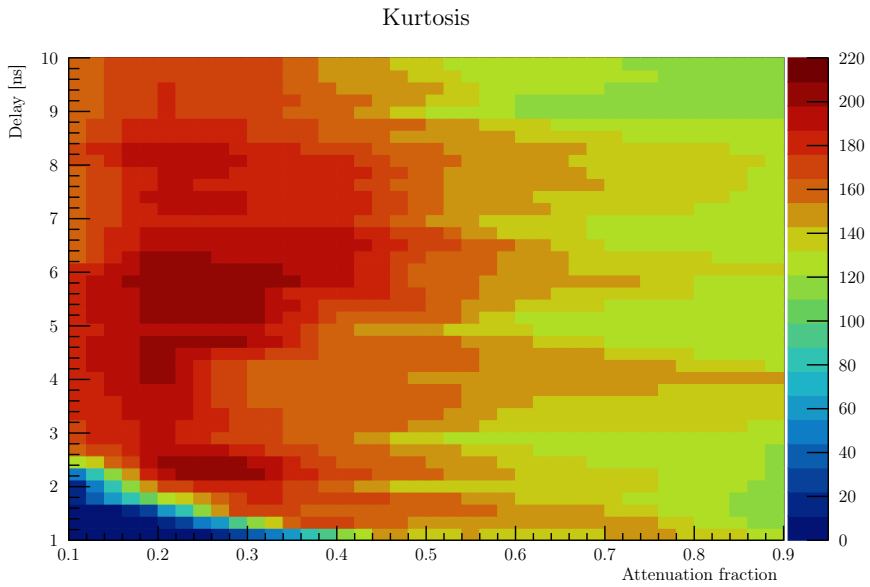

Figure 15: Kurtosis of the time differences distribution as function of CFTD parameters.

Note that the low-delay low-fraction corner points seems the best in kurtosis: on a more accurate analysis, however, their means result incompatible with the others and their sigma extremely high, reflecting errors (probably due to low digitizer time resolution) in zero-crossings finding.

The kurtosis values are very high: plotting one of the distribution, it's clear they aren't gaussian-like, but triangular-like, again because of digitizer resolution. It records only 5-6 points in the rising time, digitally sampled; the zero crossing is therefore individuated by interpolating two (or in very good conditions four) points: a very rough interpolation! Assuming the uniform probability density function (PdF) typical of digital instruments and convolving the start and stop PdF, they result in a triangular-like PdF as experimental results show.

Qui, una volta scelto il valore ottimale di delay e attenuation fraction, potremmo inserire un grafico in cui, per un solo canale alla volta, una volta allineati i picchi originali applichiamo il CFTD su tutti i campioni e poi li grafichiamo tutti in un TH2F di quelli belli colorati (capitemi, è quello che mi ha fatto fare il prof l'ultimo giorno di esperimento). Se siam stati bravi dovremmo vedere la maggior parte delle onde passare per il canale a cui abbiamo allineato i picchi inizialmente.

8.4 Time resolution and energy threshold

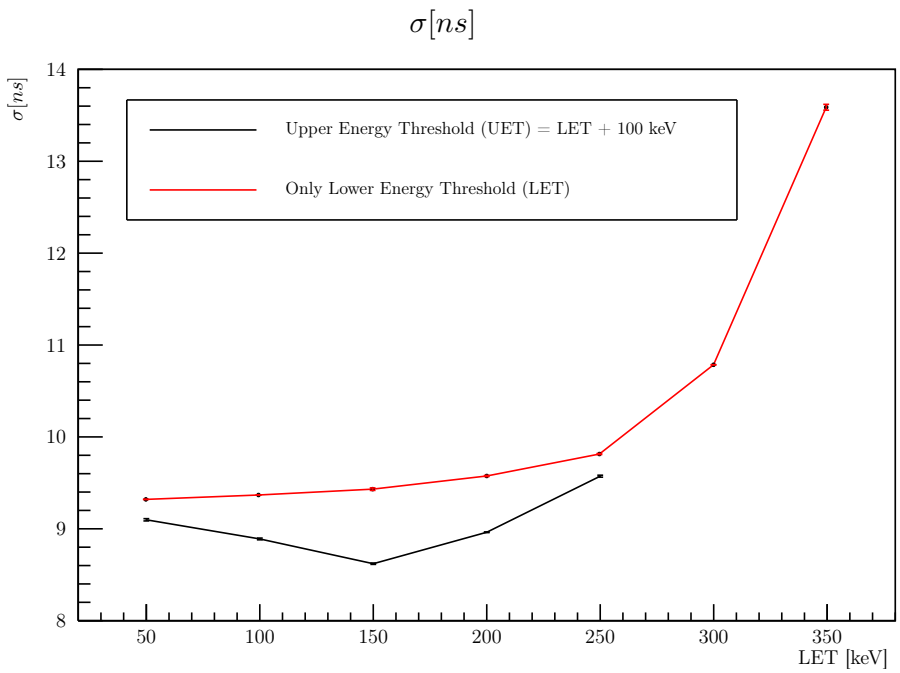

Figure 16: Sigma as a function of energy threshold.

Volendo si potrebbe fare la stessa analisi di risoluzione del Co sul sodio e confrontare la versione analogica e quella digitale

Finally, sigma has been computed varying the energy threshold, replying the procedure done for cobalt and setting the same CFTD parameters. Note that, while in the fig. 11 the low-gaussianity of the peaks lead us to compute the FWHM, here the non-gaussianity is combined with a strong white noise, which suggest us to use σ (defined as the square root of the second centered momentum, computed directly from data and without a fit). As can be seen in figure comparing fig. 11 with fig. 16, the y axis scale is different: there are about 2 order of magnitude of difference. This lead us to impute the main contribute to the sigma to the sampling done by the digitizer. In the same figure, a strong growth in sigma can be seen in high LET zone, probably due to the lack of data at high energy to make a precise mean. On the other hand, a minimum can be seen in the black line: This minimum is however not so relevant observing the σ scale.

9 Conclusions

With respect to the initial aims:

- The energy spectra has been successfully calibrated through the compton edge and the half maximum position;
- The external delay has been optimized to enhance peak sigma; the optimal delay has been found around 5ns, has theoretically expected;
- The inverse dependence of the resolution from the energy has been observed, especially for lower energies;
- The speed of light has been measured, obtaining a value compatible with the real one;
- A comparison between analogic CFD and a simulated a-posteriori ones, finding that the analogic one provide a better resolution. This result have different origins; the main one can be found in the sampling that the digitizer make, wasting precision in time and energy results.